ACS APPLIED MATERIALS & INTERFACES

Research Article

www.acsami.org

Near Infrared and Visible Luminescence from Xerogels Covalently Grafted with Lanthanide [Sm^{3+}, Yb^{3+}, Nd^{3+}, Er^{3+}, Pr^{3+}, Ho^{3+}] β-Diketonate Derivatives Using Visible Light Excitation

Lining Sun,*[,†] Yannan Qiu,[†] Tao Liu,[†] Jin Z. Zhang,[§] Song Dang,[‡] Jing Feng,[‡] Zhijuan Wang,[†] Hongjie Zhang,[‡] and Liyi Shi*[,†]

[†]Research Center of Nano Science and Technology, Shanghai University, Shanghai, Shanghai 200444, P. R. China

[‡]State Key Laboratory of Rare Earth Resource Utilization, Changchun Institute of Applied Chemistry, Chinese Academy of Sciences, Changchun, Jilin 130022, P. R. China

[§]Department of Chemistry and Biochemistry, University of California, Santa Cruz, California 95064, United States

Supporting Information

ABSTRACT: A series of ternary lanthanide β-diketonate derivatives covalently bonded to xerogels (named as Ln-DP-xerogel, Ln = Sm, Yb, Nd, Er, Pr, Ho) by doubly functionalized alkoxysilane (dbm-Si) was synthesized in situ via a sol-gel process. The properties of these xerogel materials were investigated by Fourier-transform infrared (FT-IR) spectroscopy, field-emission scanning electron microscopy (FE-SEM), diffuse reflectance (DR) spectroscopy, thermogravimetric analyses, and fluorescence spectroscopy. The data and analyses suggest that the lanthanide derivatives have been covalently grafted to the corresponding xerogels successfully. Of importance here is that, after excitation with visible light (400−410 nm), the xerogels all show characteristic visible (Sm^{3+}) as well as near-infrared (NIR; Sm^{3+}, Yb^{3+}, Nd^{3+}, Er^{3+}, Pr^{3+}, Ho^{3+}) luminescence of the corresponding Ln^{3+} ions, which is attributed to the energy transfer from the ligands to the Ln^{3+} ions via an antenna effect. Exciting with visible light is advantageous over UV excitation. Furthermore, to the best of our knowledge, it is the first observation of NIR luminescence with visible light excitation from xerogels covalently bonded with the Sm^{3+}, Pr^{3+}, and Ho^{3+} derivatives. Compared to lanthanide complexes (Ln = Er, Nd, Yb) functionalized periodic mesoporous organosilica (PMO) materials that exhibit similar optical properties reported in our previous work, the Ln-DP-xerogel (Ln = Sm, Yb, Nd, Er, Pr, Ho) in this case offer advantages in terms of ease of synthesis and handling and potentially low cost for emerging technological applications. Development of near-infrared luminescence of the lanthanide materials with visible light excitation is of strong interest to emerging applications such as chemosensors, laser systems, and optical amplifiers.

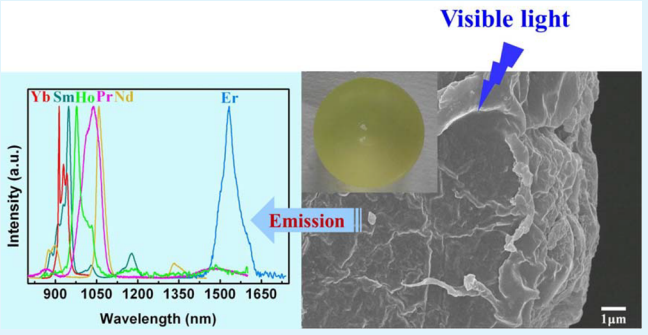

KEYWORDS: *NIR luminescent, visible-light excitation, xerogel, lanthanide β-diketonate derivatives, covalently graft*

1. INTRODUCTION

Because of the long-lived luminescent excited states and narrow emission bands, trivalent lanthanide ions are of great interest for a wide range of applications, such as tunable lasers, light-emitting diodes, low-energy scintillators, and amplifiers for optical communications, as well as in bio-science and solar energy conversion.[1,2] The emission of lanthanides spans over the entire spectrum from ultraviolet (UV) to near-infrared (NIR) regions, determined by the chemical nature of lanthanide ions, except that La^{3+} and Lu^{3+} have no luminescence. As is known, Gd^{3+} shows its emission in the UV region. Nd^{3+}, Yb^{3+}, Er^{3+}, and Ho^{3+} have NIR emission, while Eu^{3+}, Tb^{3+}, and Dy^{3+} have visible emission. (In addition, the emission of the lanthanide ions obviously depends on the high-phonon or low-phonon nature of the matrix in which the ions are embedded: for example, Er^{3+} can also show weak visible emission in low-phonon glass matrices.) The emission bands from Sm^{3+}, Pr^{3+}, and Tm^{3+} are located in both the visible and NIR regions.[3,4] Considerable research in the area of lanthanide luminescence has focused on Eu^{3+} (red color) and Tb^{3+} (green color) ions,[5−7] partly due to their high luminescence intensity as well as relatively easy-to-interpret emission spectra. In comparison with the luminescence of Eu^{3+} and Tb^{3+}, the NIR luminescence of lanthanide ions, Yb^{3+}, Nd^{3+}, and Er^{3+}, and especially Sm^{3+}, Pr^{3+}, and Ho^{3+}, is less studied but has attracted increasing attention recently. For example, Sm^{3+} is a fascinating lanthanide emitter since it shows both visible (red/orange color) and NIR luminescence. Similarly, Yb^{3+} and

Received: June 28, 2013
Accepted: September 9, 2013
Published: September 24, 2013

Ho^{3+} ions possess emission bands in the range of 0.98−1.03 μm, which is in the transparent window of biological tissues and thus of strong interest for various chemical sensing and biomedical imaging applications.[8,9] Likewise, NIR luminescence from Nd^{3+}, Er^{3+}, and Pr^{3+} proves to be very useful when employed in the laser systems and optical amplification.[1,2,9]

However, due to the strongly forbidden character of f−f transitions, the luminescence intensity of lanthanide ions is limited by its weak absorption ($\varepsilon \approx 1-10\ M^{-1}\cdot cm^{-1}$). One approach to overcoming this problem is to form complexes of lanthanide ions with chromophores that can strongly absorb light and transfer energy to the lanthanide ions (the "antenna effect"). β-Diketone ligands are well known to be efficient sensitizers, which have strong absorption over a wide wavelength range and consequently have been explored for sensitizing lanthanide ions for luminescence.[10] However, the resulting lanthanide complexes have several drawbacks for practical applications, including poor thermal stabilities and low mechanical strength.[11] Continuous efforts have been made to develop new luminescent materials with good mechanical, thermal, and chemical stability that can be easily processed. Towards this goal, sol-gel chemistry has proven to be a useful method for the development of interesting luminescent materials in which the lanthanide ions are embedded in silica xerogel.[11,12] For instance, Zhang and co-workers have reported the synthesis of lanthanide sol-gel materials by using the modified ligand of 1,10-phenanthroline, 5-(*N*,*N*-bis-3-(triethoxysilyl)propyl)ureyl-1,10-phen anthroline (phen-Si).[13−15] By using the ligand exchange reaction, Binnemans et al. have grafted several lanthanide complexes to the sol-gel matrix with the phen-Si ligand.[16−19] Yan et al. developed a series of lanthanide sol-gel materials by means of functionalized alkoxysilane as the Si−O linkage and sensitization agent.[20−23] In addition, Li et al. covalently bonded the lanthanide ionic liquid to the silica matrix via an in situ sol-gel process.[24]

Usually, the optical excitation window for the sol-gel materials containing the lanthanide derivatives is limited to UV light of <385 nm owing to the energetic constraints highlighted by Reinhoudt et al.[7,25] However, visible light is advantageous over UV excitation for these materials.[26−29] First, compared to UV excitation, excitation with visible light reduces the background fluorescence strongly. Second, excitation with visible light is less prone to the interferences by inner filter effect due to the absorption of light. Third, the damage to biological tissue is reduced with visible light compared to UV excitation. Recently, this field has attracted increasing attention because of the demand for less harmful labeling reagents for biomedical applications.

In this work, we report the successful expansion of the excitation window to the visible region for xerogels covalently grafted by lanthanide β-diketonate derivatives (named as Ln-DP-xerogel, Ln = Sm, Yb, Nd, Er, Pr, Ho), which subsequently exhibit highly efficient Ln^{3+}-centered luminescence. The xerogel materials are highly rigid and do not segregate. Upon excitation with visible light, the xerogels display the characteristic visible and NIR emission of the corresponding lanthanide ions. Although the lanthanide complexes (Ln = Er, Nd, Yb) functionalized periodic mesoporous organosilica (PMO) materials reported in our previous paper[27] and the Ln-DP-xerogel (Ln = Sm, Yb, Nd, Er, Pr, Ho) in this case are both excited by the visible light and show NIR luminescence, they are totally different materials. In the previous work, the lanthanide complexes were grafted to the PMO materials by using the synthesized silsesquioxane precursor 4,4′-bis[Si-$(OEt)_3(CH_2)_4$]-2,2′-bipyridine (bpd-Si). Following visible light excitation, the obtained three lanthanide complexes functionalized PMO materials ($Ln(dbm)_3$bpd-PMO, Ln = Er, Nd, Yb) show NIR-luminescence of the corresponding Ln^{3+} ions. While, in this case, a series of ternary lanthanide β-diketonate derivatives covalently bonded to xerogels (named as Ln-DP-xerogel, Ln = Sm, Yb, Nd, Er, Pr, Ho) by the double-functionalized alkoxysilane dbm-Si were synthesized in situ via a sol-gel process. Importantly, xerogels offer advantages over the PMO materials in terms of ease of synthesis and handling and potentially low cost for emerging technological applications. In addition, in this work, we offer a more detailed explanation about the fundamental energy transfer and relaxation mechanisms. Furthermore, to the best of our knowledge, it is the first time that, based on the visible-light excitation, the xerogel materials covalently linked with the Sm^{3+}, Pr^{3+}, and Ho^{3+} derivatives show NIR luminescence, which is highly desired for biomedical and photonics applications. A model is proposed on the basis of the relevant energy levels to explain the observed results and understand the associated fundamental energy transfer and relaxation pathways. The design principles developed can be extended and applied to other materials systems for various emerging technological applications.

2. EXPERIMENTAL SECTION

2.1. Chemicals. Tetraethoxysilane (TEOS, Aladdin), 1,10-phenanthroline mono-hydrate (phen·H_2O, 99%, Aladdin), dibenzoylmethane (Hdbm, Aladdin), 3-(triethoxysilyl)propyli-socyanate (TEPIC, Aladdin), sodium hydride (NaH, 95%, Aldrich), hydrochloric acid, *N*,*N*-dimethylformamide (DMF), and ethanol were commercially available and used without purification. The solvent tetrahydrofuran (THF) and *N*,*N*-dimethylformamide (DMF) were used after desiccation. Ytterbium oxide (Yb_2O_3, 99.99 %), samarium oxide (Sm_2O_3, 99.99%), neodymium oxide (Nd_2O_3, 99.99%), erbium oxide (Er_2O_3, 99.99%), praseodymium oxide (Pr_2O_3, 99.99%), holmium oxide (Ho_2O_3, 99.99%), and gadolinium chloride ($GdCl_3$, 99.99%) were bought from Sigma-Aldrich. Hydrated $LnCl_3$ salts (Ln = Sm, Yb, Nd, Er, Pr, Ho) were obtained by dissolving Ln_2O_3 (Ln = Sm, Yb, Nd, Er, Pr, Ho) in hydrochloric acid (HCl). The resulting solutions were evaporated with heating; the residues were again dissolved in distilled water, transferred to a volumetric flask, and diluted. The concentration of the lanthanide ion was measured by titration with a standard EDTA (ethylenediaminetetraacetic acid) aqueous solution.

2.2. Synthesis of β-Diketonate-Functionalized Alkoxy-Silane (dbm-Si). The synthesis of dbm-Si was improved according to the method in references 30−32: The dibenzoylmethane was dissolved in a suitable volume of dehydrate THF; then, NaH was added (dibenzoylmethane/NaH = 1:2, molar ratio) with stirring. Two hours later, 3-(triethoxysilyl)-propyli-socyanate (TEPIC) was added drop-wise into the refluxing solution. The molar ratio of TEPIC/dbm was 1:1. The mixture was heated at 70 °C in a covered flask for approximately 12 h in an argon atmosphere. Then, the solvent was distilled off under reduced pressure, yielding the alkoxysilane modified dibenzoylmethane: a yellow sticky solid named as dbm-Si ($C_{25}H_{33}O_6NSi$). ^1H NMR ($CDCl_3$): δ 0.58 (4H, t, CH_2Si), 1.22 (9H, q, $CH_3(OEt)$), 1.62 (2H, m, $CH_2CH_2CH_2$), 3.15 (2H, t, $NHCH_2$), 3.71−3.84 (6H, m, $SiOCH_2$), 7.2−7.4 (10H, m, $-C_6H_5$), 8.01 (1H, s, NH).

2.3. Preparation of Xerogels Grafted with Lanthanide β-Diketonate Derivatives (Denoted As Ln-DP-Xerogel, Ln = Sm, Yb, Nd, Er, Pr, Ho). The precursor dbm-Si and phen were dissolved in DMF solvent, and then, an appropriate amount of $LnCl_3$ solution was dropwise added into the above solution under stirring, respectively. TEOS, ethanol, and deionized water (acidified with HCl, pH = 2) were put in the solution by drops. The molar ratio of

dbm-Si/TEOS/H_2O/$LnCl_3$/phen is 3:187.5:750:1:1. The solution was stirred for approximately 3 h to ensure homogeneous mixing and form one single phase. Then, it was transferred to a sealed plastic container. After several days of gelation at 40 °C, the precursor solution converted to a wet gel and then continuously dried to a xerogel.

2.4. Synthesis of Gd(dbm-Si)$_3$ Complex. The dbm-Si was dissolved in anhydrous DMF (about 10 mL), and then, solid $GdCl_3$ was added to the DMF with a molar ratio of 1:3 ($GdCl_3$/dbm-Si). The mixture was reacted for 6 h under stirring at 80 °C in an argon atmosphere. After cooling by using the ice water, the precipitates were collected by filtration and washing with anhydrous DMF and dried at 80 °C under vacuum for 10 h.

2.5. Characterization. Scanning electron micrographs (SEM) were obtained by using a JSM-6700F microscope operating at 10.0 kV. Fourier-transform infrared (FT-IR) spectra were recorded in the 4000−400 cm^{-1} region on an American Thermo Nicolet Corporation model AVATAR370 FT-IR infrared spectrophotometer with the KBr pellet technique. ^1H NMR spectra were measured by a Bruker AVANCE-500 spectrometer with tetramethylsilane (TMS) as internal reference ($CDCl_3$ as solvent). The diffuse reflectance (DR) measurements were performed with a Hitachi U-4100 spectrophotometer. The excitation and emission spectra were recorded by a Edinburgh FLS920 fluorescence spectrometer equipped with a 450 W Xe-lamp as an excitation source and a monochromatoriHR320 equipped with a liquid-nitrogen-cooled R5509-72 PMT as the detector. The low-temperature phosphorescence spectrum of the Gd complex was carried out on a Hitachi F-4500 spectrophotometer at liquid nitrogen temperature. Thermogravimetry (TG) was performed on a Netzsch STA 449 at a heating rate of 10 °C·min^{-1} under air atmosphere.

3. RESULTS AND DISCUSSION

The β-diketones used as ligands for lanthanide ions have been studied in detail due to their excellent luminescence properties.[10] 1,10-Phenanthroline (phen) can serve as the synergistic agent based on its being able to prevent H_2O molecules from bonding to the Ln^{3+} ions.[10] There are a large number of hydroxyl groups (in Si−OH and H_2O) in xerogel materials, which can nonradiatively quench the luminescence of lanthanide complexes. Thus, physical mixing of the lanthanide complexes and the sol-gel matrix may cause the phase separation, inhomogeneous dispersion, and optical quenching of lanthanide ions. In our study, the double-functionalized alkoxysilane dbm-Si was prepared, which has three advantages: (1) it acts as one of the organosilane precursors for cohydrolysis and copolycondensation with TEOS to occur; (2) it can coordinate with lanthanide ions by acting as a ligand; (3) compared with modified synergic ligand, such as 1,10-phenanthroline and 4,4′-bipyridine, dbm-Si can introduce ternary β-diketonate complexes without ligand exchange reactions.[33] In this way, the lanthanide β-diketonate derivatives are suggested to be synthesized and linked to the SiO_2 backbone by dbm-Si that plays the role of organosilane precursor and sensitizing agent at the same time. The proposed structure of the Ln-DP-xerogel materials is shown in Scheme 1.

3.1. FT-IR Spectra. The FT-IR spectra of pure gel (a), dbm-Si (b), and Sm-DP-xerogel (c) are shown in Figure 1. The spectrum for the pure gel (Figure 1a) exhibits strong and broad bands in the range of 1000−1250 cm^{-1}, which are assigned to asymmetric Si−O stretching vibration modes. The peak at 794 cm^{-1} can be attributed to the symmetric Si−O stretching vibration. The Si−O−Si bending vibration observed at 461 cm^{-1} indicates the formation of the Si−O−Si framework in the silica host structure. In addition, the bands at 940 cm^{-1} can be assigned to stretching vibrations of Si−OH surface groups. In the spectrum of dbm-Si (Figure 1b), there are bands located at

Scheme 1. Proposed Structure of the Ln-DP-Xerogel (Ln = Sm, Yb, Nd, Er, Pr, Ho)

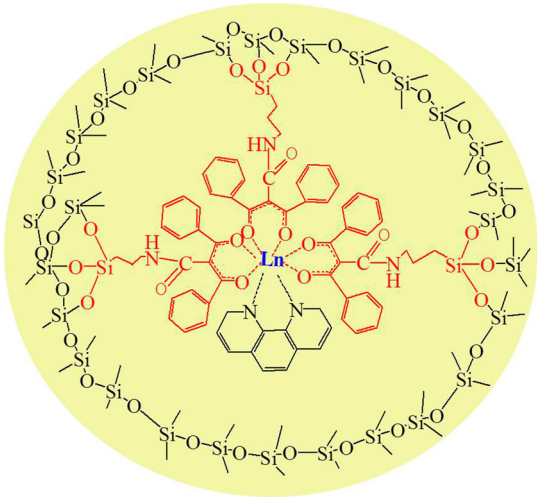

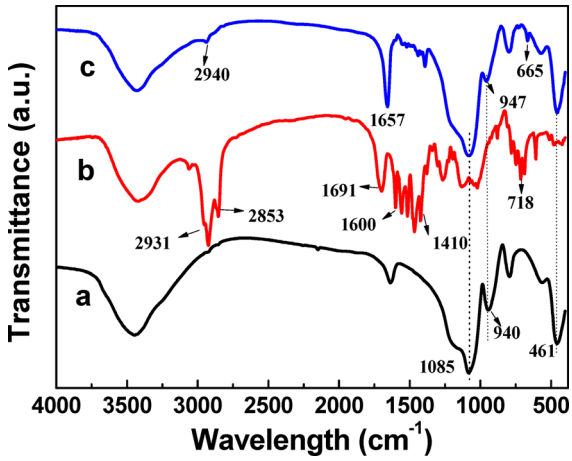

Figure 1. FT-IR spectra of the pure gel (a), dbm-Si (b), and Sm-DP-xerogel (c).

around 2931 cm^{-1}, which are derived from the three methylene groups of cross-linking reagent TEPIC. The bands centered at 1691 cm^{-1} suggest the formation and retaining of the C═O bond in the dbm-Si. Furthermore, several bands at around 1410−1600 cm^{-1} are apparent and attributed to the breathing vibration of benzene ring from dbm-Si derivates. Compared with the spectrum of the silica host structure (Figure 1a), the spectrum for the Sm-DP xerogel (Figure 1c) exhibits similar bands which indicate homologous Si−O−Si structure formed. The characteristic bands of dbm-Si in the spectrum for the Sm-DP xerogel (Figure 1c) suggest that dbm-Si was successfully incorporated into the xerogel, though less prominent compared with Figure 1c. This is possibly due to the low concentration of dbm-Si in the Sm-DP xerogel matrix (dbm-Si/TEOS = 1.5 mol %). The FT-IR spectra of other Ln-DP-xerogel (Ln = Yb, Nd, Er, Pr, Ho) are quite similar to that of Sm-DP-xerogel, which are presented in Figures S1−S5, Supporting Information. In all, FT-IR results suggest the in situ synthesis of lanthanide derivatives in the Ln-DP-xerogel (Ln = Sm, Yb, Nd, Er, Pr, Ho).

3.2. Scanning Electron Microscopy (SEM). Figure 2 shows representative SEM images and photographs (inset) of the Yb-DP-xerogel and Nd-DP-xerogel. The SEM images are

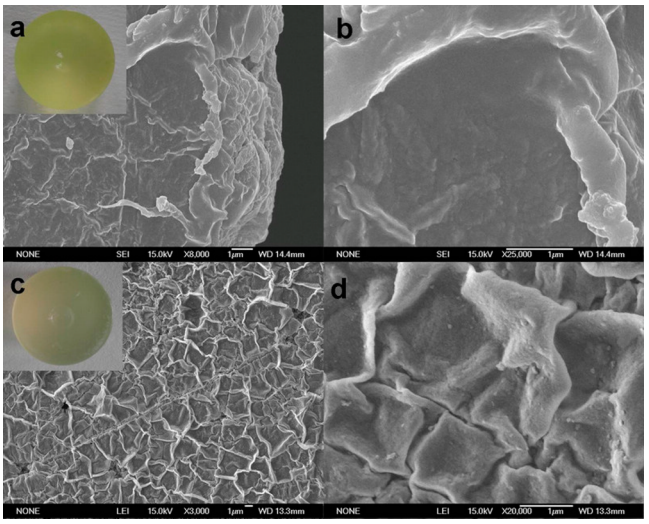

Figure 2. SEM images of Yb-DP-xerogel (a, b) and Nd-DP-xerogel (c, d), the insets of a and c show the pictures of the xerogels of Yb-DP-xerogel and Nd-DP-xerogel, respectively.

similar for other Ln-DP-xerogel (Ln = Sm, Er, Pr, Ho). The Ln-DP-xerogel materials with the shape of the reaction vessel are transparent and rigid and show no cracks (see Figure 2, insets). The SEM images of Yb-DP-xerogel show a spiral chain-like morphology that looks like a cobweb network, which is highly homogeneous and exhibits no segregation even at a high magnification of 25 000 (Figure 2b). Changing the Ln^{3+} ion has little influence on the microstructure, since the SEM image of Nd-DP-xerogel (Figure 2c) is very similar to that of the Yb-DP-xerogel. This may be because the microstructures of the hybrid xerogels mainly depend on the sol-gel process, which is influenced by temperature, pH value, and aging time.[23] The uniform morphology of these hybrid materials demonstrates that a self-assembly process might have happened during the co-condensation of dbm-Si and TEOS. It is a consequence of the doubly functionalized alkoxysilane precursor dbm-Si that covalently bonds the lanthanide complexes to the xerogel Si−O−Si networks. In this case, it can be attributed to the in situ synthesis technique used and the strong covalent bonds linking the organic and inorganic phases, by which all the components are homogeneously blended at the molecular level. Therefore, the xerogels are highly uniform organic−inorganic hybrid materials.[28]

3.3. Diffuse Reflectance (DR). Representative DR spectra of Ho-DP-xerogel and Nd-DP-xerogel are shown in Figure 3. The DR spectra of other Ln-DP-xerogel (Ln = Sm, Yb, Er, Pr) are displayed in Figures S6−S9, Supporting Information. The spectra all exhibit broad absorption bands in the range from 200 to 400 nm, which likely correspond to electronic transitions from the ground state (π) S_0 to the excited state (π^*) S_1 of the ligands. In the visible and NIR region of these spectra, each absorption band is associated with the characteristic transition between two spin−orbit coupling levels of the corresponding lanthanide ions. In Figure 3a, the peaks at 451, 485, 538, 643, 821, and 1186 nm are assigned to the transitions from the ground level $^5I_8$ to excited levels $^5G_6 + {}^5F_1$, $^5F_3$, $^5F_4$, $^5F_5$, $^5I_5$, and $^5I_6$ of the Ho^{3+} ion,[34,35] respectively. Similarly, the absorption bands observed in Figure 3b at 512, 524, 582, 680, 745, 800, and 863 nm are attributed to the Nd^{3+} transitions of $^4G_{9/2} \leftarrow {}^4I_{9/2}$ (ground state), $^4G_{7/2} + {}^2K_{13/2} \leftarrow {}^4I_{9/2}$, $^2G_{7/2} \leftarrow {}^4I_{9/2}$, $^4F_{9/2} \leftarrow {}^4I_{9/2}$, $^4F_{7/2} \leftarrow {}^4I_{9/2}$, $^4F_{5/2} \leftarrow {}^4I_{9/2}$, and $^4F_{3/2} \leftarrow {}^4I_{9/2}$, respectively.[36]

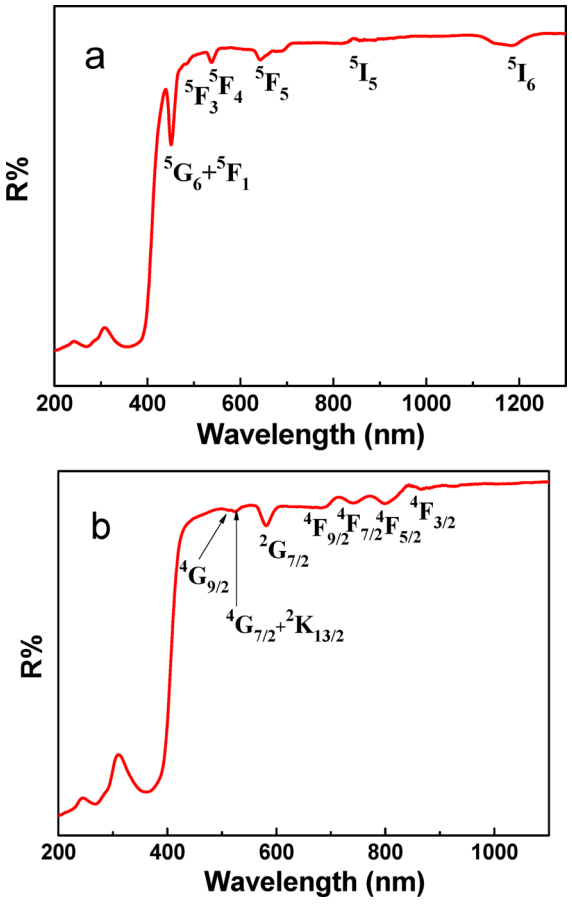

Figure 3. DR spectra of Ho-DP-xerogel (a) and Nd-DP-xerogel (b).

3.4. Photoluminescence Studies. Figure 4 shows the photoluminescence (PL) spectra of Sm-DP-xerogel. The PL excitation spectrum was obtained by monitoring the emission wavelength of Sm^{3+} ion at 646 nm and recorded at room temperature. The spectrum exhibits a broad band in the UV/visible region from 200 to 450 nm, which is due to absorption by the organosilane dbm-Si and phen ligands. The PL excitation spectrum monitored at the emission wavelength of 947 nm was almost the same as that monitored at 646 nm (not given here). For the PL spectra, the excitation wavelength was set at 410 nm that extends to the visible region, and the energy could be absorbed by the ligands and transferred to the Sm^{3+} emitting center by the antenna effect.[27] The emitting level for the visible emission (Figure 4a) is the $^4G_{5/2}$ level, and the emission peaks correspond to transitions from the $^4G_{5/2}$ level to the different ^6H_J levels (J = 5/2, 7/2, 9/2, 11/2).[37−39] The strongest transition (645 nm) in the visible region is the hypersensitive $^4G_{5/2} \rightarrow {}^6H_{9/2}$ transition. The transition responsible for the 560 nm emission, $^4G_{5/2} \rightarrow {}^6H_{5/2}$, has a predominant magnetic dipole character.[40,41] The intensity ratio of $I(^4G_{5/2} \rightarrow {}^6H_{9/2})/I(^4G_{5/2} \rightarrow {}^6H_{5/2})$ can be used as a measure for the polarizability of the chemical environment of the Sm^{3+} ion.[42] All the emissions of Sm-DP-xerogel in the NIR range also come from the $^4G_{5/2}$ excited state, as shown in Figure 4b, and the most intense transition at 947 nm is assigned to $^4G_{5/2} \rightarrow {}^6F_{5/2}$ transition.[43]

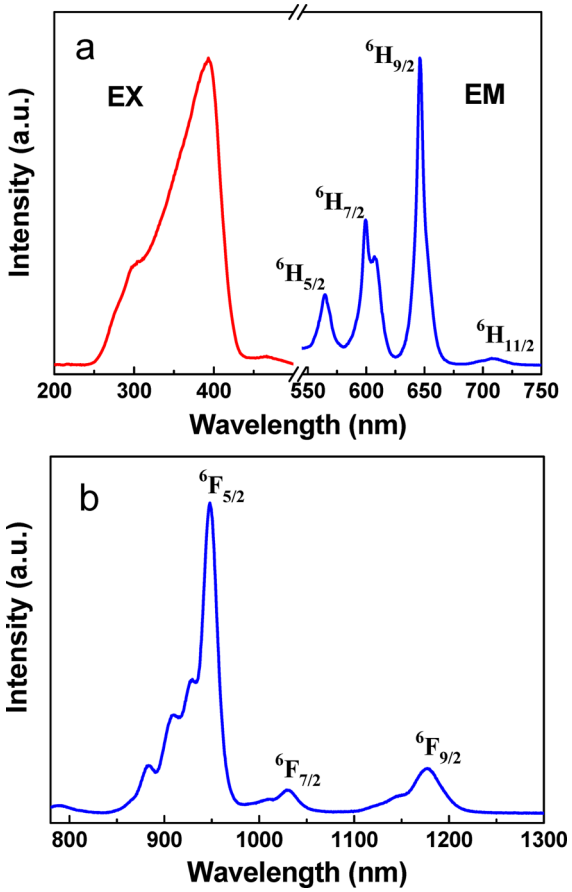

Figure 4. Fluorescence spectra for the Sm-DP-xerogel material: (a) excitation (λ_{em} = 646 nm) and visible emission (λ_{ex} = 410 nm) spectra; (b) emission (λ_{ex} = 410 nm) spectrum in the NIR region.

The PL spectra of Yb-DP-xerogel are shown in Figure 5. The PL excitation spectrum was measured by monitoring the

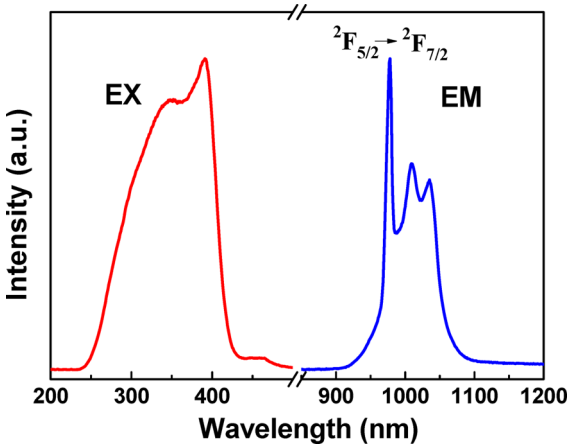

Figure 5. Excitation (λ_{em} = 980 nm) and emission (λ_{ex} = 401 nm) spectra for the Yb-DP-xerogel material.

strongest emission wavelength of Yb^{3+} ion. The key feature is a broad band ranging from 200 to 450 nm, which can be assigned to the absorption of the dbm-Si and phen ligands. Upon excitation with visible light, the NIR emission spectrum of the Yb-DP-xerogel was obtained, as shown in Figure 5. It shows the characteristic luminescence of the Yb^{3+} ion, and the bands in the region of 906−1110 nm with a sharp peak at 980 nm is assigned to the $^2F_{5/2} \rightarrow {}^2F_{7/2}$ transition, with broader vibronic components at longer wavelength.[27,44] It should be noticed that the emission of Yb-DP-xerogel is not a single sharp band but rather quite broad, which may be caused by the splitting of the energy levels of Yb^{3+} ion as a result of ligand field effect.[28,45] The Yb^{3+} ion has been proven very useful in lasers and optical amplifiers for several important reasons:[46] (1) it has a relatively broad absorption (compared with other Ln^{3+} ions); (2) it possesses very simple energy level structure (the $^2F_{7/2}$ ground state and the $^2F_{5/2}$ excited state), with no excited-stated absorption, little reduction on the effective laser cross-section, no concentration quenching, and no absorption in the visible range;[35] and (3) the Yb^{3+} ion could transfer energy to other lanthanide ions, like Pr^{3+} ion,[47] Er^{3+} ion,[48] and Tm^{3+} ion.[49] Furthermore, Yb-based NIR emission (around 980 nm) is of interest for biomedical applications because of deeper tissue penetration and no competing fluorescence from biomatrices.[50]

The PL spectra of the Nd-DP-xerogel are shown in Figure 6. In the PL excitation spectrum, a broad band (260−550 nm)

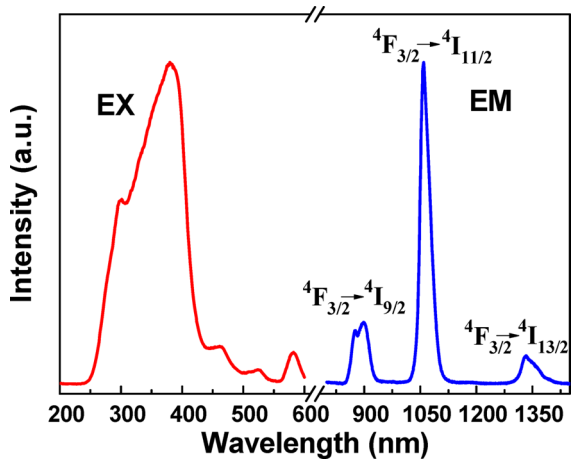

Figure 6. Excitation (λ_{em} = 1060 nm) and emission (λ_{ex} = 401 nm) spectra for the Nd-DP-xerogel material.

was observed when monitored by the emission of Nd^{3+} ion at 1060 nm, being assigned to the absorption of the ligands. Several bands characteristic of the Nd^{3+} ion can be assigned to the $^2K_{13/2} + {}^4G_{7/2} \leftarrow {}^4I_{9/2}$ (525 nm) and $^2G_{7/2} \leftarrow {}^4I_{9/2}$ (582 nm) transitions,[35,51] in line with the DR result (see Figure 3b). It should be noticed that the absorption transitions of Nd^{3+} ion are much weaker than that of the ligands, so exciting the absorption of ligands is much more efficient than direct excitation of the absorption of Nd^{3+}ion. With photoexcitation at 401 nm, the PL spectrum of Nd-DP-xerogel shown in Figure 6 consists of three emission bands peaked at 900, 1060, and 1333 nm, assigned to the f−f transitions of $^4F_{3/2}$ (emitting level) $\rightarrow {}^4I_{9/2}$, $^4F_{3/2} \rightarrow {}^4I_{11/2}$, and $^4F_{3/2} \rightarrow {}^4I_{13/2}$, respectively.[36,44] The emission at 1060 nm is the most strongest, which is possibly useful for laser applications. The emission band at 1335 nm is potentially useful for optical amplification at 1.3 μm, an important spectral window for optical telecommunication.[52,53]

The PL excitation spectrum of the Er-DP-xerogel, similar to those of xerogels mentioned above, also shows broad bands from 200 to 450 nm, which can be assigned to the $\pi-\pi^*$ electron transition of the ligands (Figure 7). A weaker band, originating from the f−f absorption transition $^2H_{11/2} \leftarrow {}^4I_{15/2}$

dx.doi.org/10.1021/am402529w | ACS Appl. Mater. Interfaces 2013, 5, 9585−9593

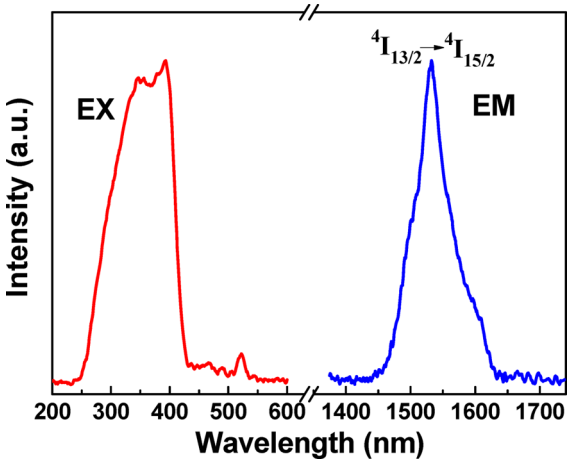

Figure 7. Excitation (λ_{em} = 1535 nm) and emission (λ_{ex} = 401 nm) spectra for the Er-DP-xerogel material.

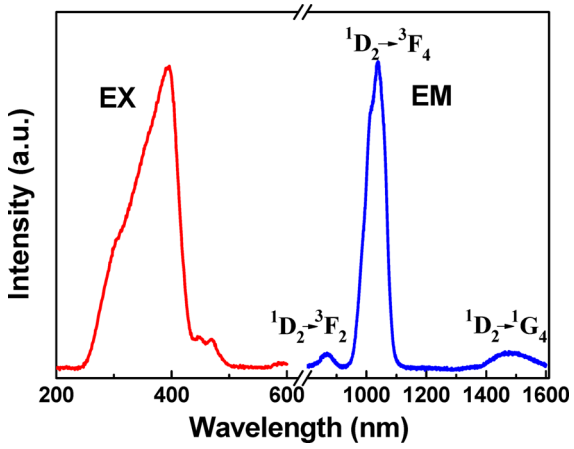

Figure 8. Excitation (λ_{em} = 1040 nm) and emission (λ_{ex} = 401 nm) spectra for the Pr-DP-xerogel material.

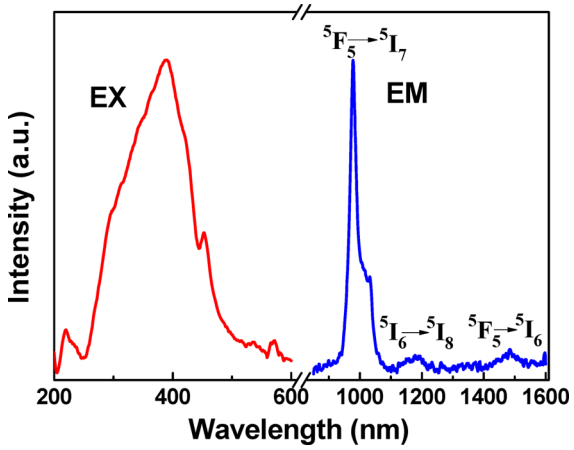

Figure 9. Excitation (λ_{em} = 978 nm) and emission (λ_{ex} = 401 nm) spectra for the Ho-DP-xerogel material.

(521 nm) of the Er^{3+} ion, is observed in the excitation spectrum,[35] consistent with the DR spectrum (Figure S8, Supporting Information). Since this absorption transition is much weaker than that of the ligands (dbm-Si and phen), sensitization the luminescence of lanthanide derivate by exciting the ligands absorption is much more efficient than directly exciting the absorption of Er^{3+} ion. The PL emission spectrum, centered at 1535 nm, was obtained by exciting the ligands (λ_{ex} = 401 nm). The emission band covers a broad spectral range, from 1450 to 1650 nm, and is attributed to the $^4I_{13/2} \rightarrow {}^4I_{15/2}$ transition of Er^{3+} ion.[54−58] The erbium doped materials attract much interest in application of optical amplification because the emission band around 1.54 μm is in the desired region for the third telecommunication window.[59−61] In order to obtain a wide gain bandwidth for optical amplification, a broad emission band is desirable. The full width at half maximum of the transition $^4I_{13/2} \rightarrow {}^4I_{15/2}$ of the Er-DP-xerogel is 65 nm, which may endow a wide gain bandwidth for optical amplification.

Compared with other lanthanide ions, the PL spectrum of Pr^{3+} ion is more complicated, since the Pr^{3+} ion can display luminescent peaks from three levels ($^3P_0$, $^1D_2$, and $^1G_4$) after exciting the absorption of organic ligands. It is of interest to obtain the NIR luminescence of Pr^{3+} ion in the Pr-DP-xerogel with the visible-light excitation, as shown in Figure 8. In the PL excitation spectrum, there are two weak bands, at 450 and 469 nm, attributed to f−f absorption transitions $^3P_2 \leftarrow {}^3H_4$ and $^1I_6 \leftarrow {}^3H_4$ of the Pr^{3+} ion, which is in agreement with the DR spectrum (Figure S9, Supporting Information). In the emission spectrum, the band around 1038 nm originates from $^1D_2$ to $^3F_4$ transition, since the $^1G_4 \rightarrow {}^3H_5$ emission around 1320 nm was not observed, suggesting that the nonradiative process with phonon assistance dominates the relaxation of $^1G_4$ energy levels. Thus, the emission at 1038 nm originates from $^1D_2$, instead of $^1G_4$.[40,62] The emission bands at 868, 1038, and 1476 nm are ascribed to $^1D_2 \rightarrow {}^3F_2$, $^1D_2 \rightarrow {}^3F_4$, and $^1D_2 \rightarrow {}^1G_4$ transitions of the Pr^{3+} ion, respectively.[62−65]

Figure 9 presents the PL excitation and emission spectra of the Ho-DP-xerogel. In the PL excitation spectrum, a broad band in the UV/vis region is observed, which can be attributed to the absorption of the ligands. The excitation edge of the ligand overlaps with an absorption peak (453 nm) corresponding to the characteristic transition of the Ho^{3+} ion ($^5G_6 + {}^5F_1 \leftarrow {}^5I_8$), which is consistent with the DR spectrum (Figure 3a). Excitation of the ligands absorption band with visible light (λ_{ex} = 401 nm) and the emission spectrum of the Ho-DP-xerogel can be obtained (Figure 9). In this case, the PL spectrum consists of three bands centered at 977, 1200, and 1500 nm, which are attributed to the f−f transitions of $^5F_5 \rightarrow {}^5I_7$, $^5I_6 \rightarrow {}^5I_8$, and $^5F_5 \rightarrow {}^5I_6$, respectively.[34,35,66] As the optimal energy difference favors efficient energy transfer from ligands to ions, it is supposed that the levels of $^5F_4$, $^5S_2$, and $^5F_5$ are the main acceptor levels, and the excited electrons on the levels of $^5F_5$ and $^5I_6$ could come from the relaxation of the upper levels partially followed by the transitions to the lower levels, resulting in the emissions of Ho^{3+} ion.[67] Among the observed three emissions of the emission spectrum, the intensity of the emission band at 977 nm is most strongest, which is probably useful in biomedical applications. In the meantime, the emission band at 1500 nm could be a suitable candidate for the optical communication applications.[35,62,68]

3.5. Mechanism of Energy Transfer. As described above, because the f−f transitions in the lanthanide ions are forbidden, the intensities of absorption bands are usually weak. The indirect excitation by energy transfer from the sensitizer not only circumvents this absorption problem but also allows excitation at wavelength where the lanthanide ions do not show absorption.[56] Because no absorption of the lanthanide ions

Scheme 2. Schematic Illustration for the Primary Energy Transfer Pathways in the Visible Light Sensitization Process (Left) and Diagram of the 4f Energy Levels of Sm^{3+}, Yb^{3+}, Nd^{3+}, Er^{3+}, Pr^{3+}, and Ho^{3+} Ions (Right)

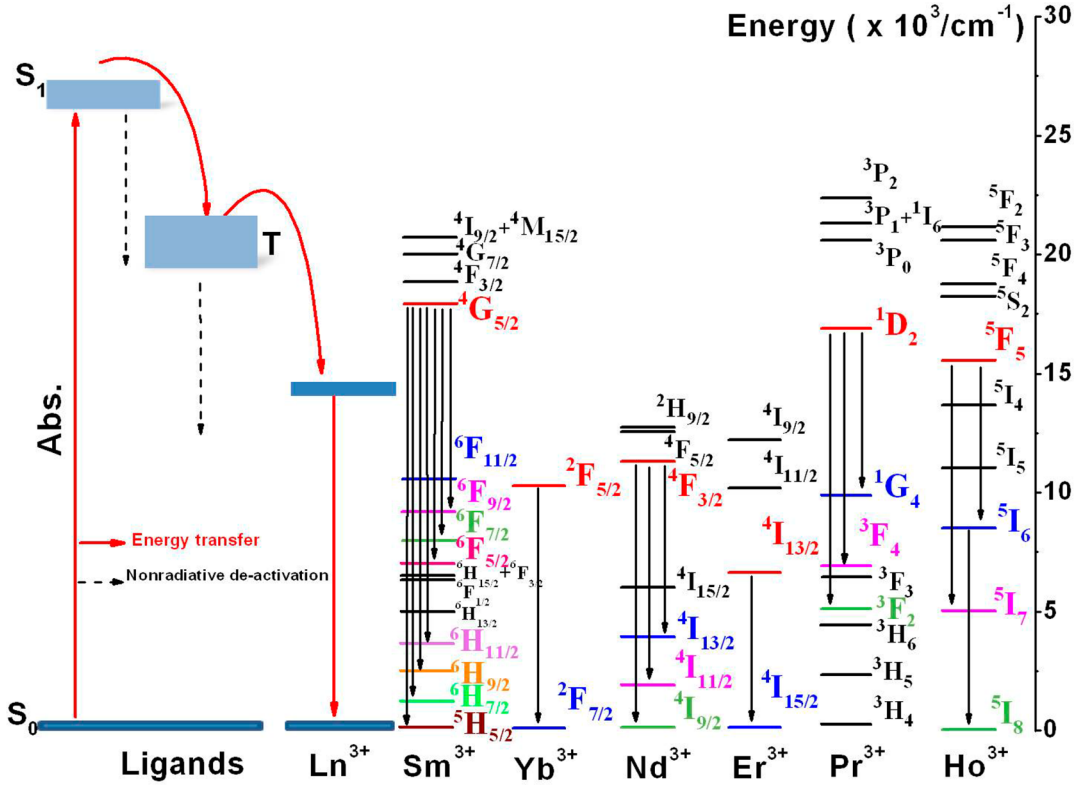

occurs with visible excitation wavelengths (410 nm for Sm-DP-xerogel, 401 nm for Yb-DP-xerogel, Nd-DP-xerogel, Er-DP-xerogel, Pr-DP-xerogel, and Ho-DP-xerogel), the observed vis/NIR emission can only originate from the lanthanide ions sensitized by the ligands moiety. In this case, the triplet-state energy level of dbm-Si ligand was studied by using the phosphorescence spectrum of Gd complex and calculated to be 20 240 cm^{-1} (Figure S10 in Supporting Information). Upon excitation with visible light at the absorption of the organic ligands, we obtained the lanthanide ion emission in the Ln-DP-xerogels. This indicates that (1) the triplet states of the ligands could match well with the lanthanide ions; (2) ligands are able to transfer the absorbed visible light to the lanthanide ions via the antenna effect; (3) the corresponding complexes are formed between lanthanide ions and the ligands, which are attached to the silica matrix in Ln-DP-xerogel.[69]

The obtained vis/NIR luminescence in this case illustrates that the ligands shield the lanthanide ions well from the surroundings and intramolecular energy transfer does occur between the ligands and the lanthanide ions. To help explain and understand the observed spectral results, a schematic diagram is shown in Scheme 2 to illustrate the primary energy levels involved and major energy transfer and relaxation pathways during the sensitization of lanthanide luminescence via the ligands. In particular, a scheme of 4f energy levels of Sm^{3+}, Yb^{3+}, Nd^{3+}, Er^{3+}, Pr^{3+}, and Ho^{3+} ions is shown in detail on the right of the Scheme 2. The electrons of the ligands are first excited from the singlet S_0 ground state to the singlet S_1 excited state by absorbing visible light. The energy of S_1 excited state is then transferred to the triplet excited state (T) of the ligands through intersystem crossing. Competing processes include ligand fluorescence and nonradiative de-activation of the excited singlet. Subsequently, the excitation energy is transferred to the 4f states of lanthanide ions, which ultimately result in the corresponding lanthanide ion emission of interest.[3]

3.6. Thermogravimetric Analysis. To investigate the thermal stability of the Ho-DP-xerogel hybrid materials, thermogravimetric analysis (TGA) was performed at a heating rate of 10.0 °C·min^{-1}. The TGA diagrams of other Ln-DP-xerogel materials are quite similar to that of the Ho-DP-xerogel, which is given as an example. Figure 10 shows the thermogravimetric (TG) weight loss curve and differential scanning calorimetry (DSC) curves of the Ho-DS-P-Gel under air atmosphere. There are three main degradation steps: the first weight loss from 42 to 274 °C gives loss of 25.59%, corresponding to the loss of physically absorbed water and residual organic solvent and water. This was followed by a

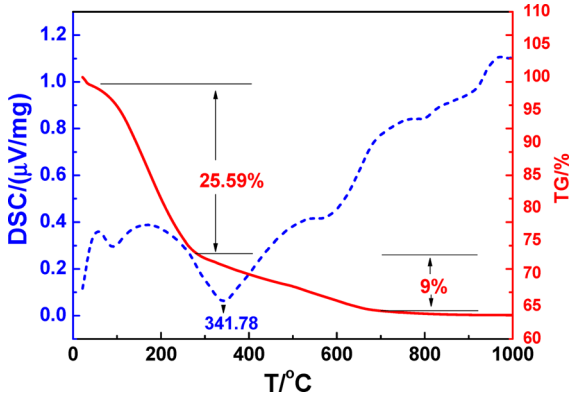

Figure 10. The TG and DSC curves of the Ho-DP-xerogel material.

dx.doi.org/10.1021/am402529w | ACS Appl. Mater. Interfaces 2013, 5, 9585−9593

second weight loss of about 9% between 274 and 700 °C, which is ascribed to the loss of coordinated water and the organic Ln^{3+} complex. Related to this, the DSC curve shows that there is an obvious endothermic peak at about 341°C. The slight weight loss beyond 700 °C may be ascribed to the release of H_2O formed from the further condensation of silanols in the silica framework, because the terminal Si−OH groups on the silica surface could undergo condensation to form Si−O−Si when temperature increases. All the other Ln-DP-xerogels (Ln = Sm, Yb, Nd, Er, Pr, Ho) present similar trends in weight loss, and the TG and DSC or DTA curves are shown in Figures S11−S15, Supporting Information.

4. CONCLUSION

In summary, Ln-DP-xerogels (Ln = Sm, Yb, Nd, Er, Pr, Ho) have been successfully synthesized and covalently linked with lanthanide/β-diketonate derivatives using doubly functionalized alkoxysilane dbm-Si. The Ln-DP-xerogel (Ln = Sm, Yb, Nd, Er, Pr, Ho) materials are highly homogeneous with no crack as revealed by SEM study and display visible as well as NIR luminescence under visible light excitation. It is worth noting that the NIR emission of Sm^{3+}, Pr^{3+}, and Ho^{3+} xerogel materials with visible light excitation is new and highly desired due to its potential applications in areas including optical amplification, medical diagnostic probe, and lasers. In addition, analysis of the data suggests some unique and useful pathways for energy transfer in this type of material that are stable and easy to synthesis and have potentially a low cost, rendering them ideally suited for technological applications.

■ ASSOCIATED CONTENT

Supporting Information

The FT-IR measurement of the Ln-DP-xerogel (Ln = Yb, Nd, Er, Pr, Ho). The DR spectra of Ln-DP-xerogel (Ln = Sm, Yb, Er, Pr). The emission spectrum of Gd(dbm-Si)$_3$ complex. The TGA diagrams of Ln-DP-xerogels (Ln = Sm, Yb, Nd, Er, Pr). This material is available free of charge via the Internet at http://pubs.acs.org.

■ AUTHOR INFORMATION

Corresponding Authors

*E-mail: lnsun@shu.edu.cn (L. N. Sun).
*E-mail: shiliyi@shu.edu.cn (L. Y. Shi).

Notes

The authors declare no competing financial interest.

■ ACKNOWLEDGMENTS

The authors thank the National Natural Science Foundation of China (Grant Nos. 21001072 and 21231004), Innovation Program of Shanghai Municipal Education Commission (13ZZ073), the Key Subject of Shanghai Municipal Education Commission (J50102), Shanghai Sci. Tech. Comm. (13NM1401100, 13NM1401101), and State Key Laboratory of Rare Earth Resource Utilization (RERU2011012). J.Z.Z. is grateful to the US NSF and the BES Division of the US DOE for financial support.

■ REFERENCES

(1) Bünzli, J.-C. G.; Eliseeva, S. V. *J. Rare Earths* **2010**, *28*, 824−842.
(2) Carlos, L. D.; Ferreira, R. A. S.; de Zea Bermudez, V.; Julián-López, B.; Escribano, P. *Chem. Soc. Rev.* **2011**, *40*, 536−549.
(3) Bünzli, J.-C. G.; Piguet, C. *Chem. Soc. Rev.* **2005**, *34*, 1048−1077.
(4) Bünzli, J.-C. G. *Acc. Chem. Res.* **2006**, *39*, 53−61.
(5) Chen, M.; Xie, L.; Li, F.; Zhou, S.; Wu, L. *ACS Appl. Mater. Interfaces* **2010**, *2*, 2733−2737.
(6) Li, G.; Zhang, Y.; Geng, D.; Shang, M.; Peng, C.; Cheng, Z.; Lin, J. *ACS Appl. Mater. Interfaces* **2012**, *4*, 296−305.
(7) de Faria, E. H.; Nassar, E. J.; Ciuffi, K. J.; Vicente, M. A.; Trujillano, R.; Rives, V.; Calefi, P. S. *ACS Appl. Mater. Interfaces* **2011**, *3*, 1311−1318.
(8) Bünzli, J.-C. G. *Chem. Rev.* **2010**, *110*, 2729−2755.
(9) Bünzli, J.-C. G. *Chem.Soc.Rev.* **2010**, *39*, 189−227.
(10) Binnemans, K. In *Handbook on the Physics and Chemistry of Rare Earths*; Elsevier Science B.V.: Amsterdam, 2005; Vol. *35*, pp 107−272.
(11) Feng, J.; Zhang, H. J. *Chem. Soc. Rev.* **2013**, *42*, 387−410.
(12) Binnemans, K. *Chem. Rev.* **2009**, *109*, 4283−4374.
(13) Li, H. R.; Lin, J.; Zhang, H. J.; Fu, L. S.; Meng, Q. G.; Wang, S. B. *Chem. Mater.* **2002**, *14*, 3651−3655.
(14) Li, H. R.; Lin, J.; Zhang, H. J.; Li, H. C.; Fu, L. S.; Meng, Q. G. *Chem. Commun.* **2001**, 1212−1213.
(15) Sun, L. N.; Zhang, H. J.; Yu, J. B.; Meng, Q. G.; Liu, F. Y.; Peng, C. Y. *J. Photochem. Photobiol., A* **2008**, *193*, 153−160.
(16) Lenaerts, P.; Ryckebosch, E.; Driesen, K.; Van Deun, R.; Nockemann, P.; Görller-Walrand, C.; Binnemans, K. *J. Lumin.* **2005**, *114*, 77−84.
(17) Binnemans, K.; Lenaerts, L.; Driesen, K.; Görller-Walrand, C. *J. Mater. Chem.* **2004**, *14*, 191−195.
(18) Lenaerts, P.; Storms, A.; Mullens, J.; D'Haen, J.; Görller-Walrand, C.; Binnemans, K.; Driesen, K. *Chem. Mater.* **2005**, *17*, 5194−5201.
(19) Lenaerts, P.; Driesen, K.; Van Deun, R.; Binnemans, K. *Chem. Mater.* **2005**, *17*, 2148−2154.
(20) Yan, B.; Zhao, L. M.; Wang, X. L.; Zhao, Y. *RSC Adv.* **2011**, *1*, 1064−1074.
(21) Yan, B.; Guo, M.; Qiao, X. F. *Photochem. Photobiol.* **2011**, *87*, 786−794.
(22) Guo, L.; Yan, B.; Liu, J. L.; Sheng, K.; Wang, X. L. *Dalton Trans.* **2011**, *40*, 632−638.
(23) Liu, J. L.; Yan, B. *Dalton Trans.* **2011**, *40* (9), 1961−1968.
(24) Feng, Y.; Li, H. R; Gan, Q. Y.; Wang, Y. E.; Liu, B. Y.; Zhang, H. J. *J. Mater. Chem.* **2010**, *20*, 972−975.
(25) Steemers, F. J.; Verboom, W.; Reinhoudt, D. N.; van der Tal, E.B.; Verhoeven, J. W. *J. Am. Chem. Soc.* **1995**, *117*, 9408−9414.
(26) Peng, H. S.; Stich, M. I. J.; Yu, J. B.; Sun, L.N.; Fischer, L. H.; Wolfbeis, O. S. *Adv. Mater.* **2010**, *22*, 716−719.
(27) Sun, L. N.; Mai, W. P.; Dang, S.; Qiu, Y. N.; Deng, W.; Shi, L. Y.; Yan, W.; Zhang, H. J. *J. Mater. Chem.* **2012**, *22*, 5121−5127.
(28) Sun, L. N.; Dang, S.; Yu, J. B.; Feng, J.; Shi, L.Y.; Zhang, H. J. *J. Phys. Chem. B* **2010**, *114*, 16393−16397.
(29) Yang, C.; Fu, L. M.; Wang, Y.; Zhang, J. P.; Wong, W. T.; Ai, X. C.; Qiao, Y.-F.; Zou, B.-S.; Gui, L.-L. *Angew. Chem., Int. Ed.* **2004**, *43*, 5010−5013.
(30) Li, K. L.; Yan, B.; Li, Y. *J. Solid State Chem.* **2009**, *182*, 1631−1637.
(31) Yan, B.; Li, Y. Y. *Dalton Trans.* **2010**, *39*, 1480−1487.
(32) DeOliveira, E.; Neri, C. R.; Serra, O. A.; Prado, A. G. S. *Chem. Mater.* **2007**, *19*, 5437−5442.
(33) Guo, X. M.; Guo, H.; Fu, L. S; Zhang, H. J.; Carlos, L. D.; Deng, R. P.; Yu, J. *J. Photochem. Photobiol., A* **2008**, *200*, 318−324.
(34) Dang, S.; Sun, L. N.; Zhang, H. J.; Guo, X. M.; Li, Z. F.; Feng, J.; Guo, H. D.; Guo, Z. Y. *J. Phys. Chem. C* **2008**, *112*, 13240−13247.
(35) Sun, L. N.; Yu, J. B.; Zheng, G. L.; Zhang, H. J.; Meng, Q. G.; Peng, C. Y.; Fu, L. S.; Liu, F. Y.; Yu, Y. N. *Eur. J. Inorg. Chem.* **2006**, 3962−3973.
(36) Feng, J.; Yu, J.-B.; Song, S.-Y.; Sun, L.-N.; Fan, W.-Q.; Guo, X.-M.; Dang, S.; Zhang, H.-J. *Dalton Trans.* **2009**, No. 13, 2406−2414.
(37) Gouveia-Neto, A. S.; da Silva, A. F.; Bueno, L. A.; da Costa, E. B. *J. Lumin.* **2012**, *132*, 299−304.
(38) Chu, B.; Li, W. L.; Hong, Z. R.; Zang, F. X.; Wei, H. Z.; Wang, D. Y.; Li, M. T.; Lee, C. S.; Lee, S. T. *J. Phys. D: Appl. Phys.* **2006**, *39*, 4549−4552.

(39) Deng, R. P.; Yu, J. B.; Zhang, H. J.; Zhou, L.; Peng, Z. P.; Li, Z. F.; Guo, Z. Y. *Chem. Phys. Lett.* **2007**, *443*, 258−263.
(40) Sun, L.-N.; Yu, J.-B.; Zhang, H.-J.; Meng, Q.-G.; Ma, E.; Peng, C.-Y.; Yang, K.-Y. *Microporous Mesoporous Mater.* **2007**, *98*, 156−165.
(41) Lunstroot, K.; Nockemann, P.; Van Hecke, K.; Van Meervelt, L.; Görller-Walrand, C.; Binnemans, K.; Driesen, K. *Inorg. Chem.* **2009**, *48*, 3018−3026.
(42) Brito, H. F.; Malta, O. L.; Felinto, M. C. F. C.; Teotonio, E. E. S.; Menezes, J. F. S.; Silva, C. F. B.; Tomiyama, C. S.; Carvalho, C. A. A. *J. Alloys Compd.* **2002**, *344*, 293−297.
(43) Sun, L.-N.; Zhang, Y.; Yu, J.-B.; Peng, C.-Y.; Zhang, H.-J. *J. Photochem. Photobiol., A* **2008**, *199*, 57−63.
(44) Moore, E. G.; Xu, J.; Dodani, S. C.; Jocher, C. J.; D'Aléo, A.; Seitz, M.; Raymond, K. N. *Inorg. Chem.* **2010**, *49*, 4156−4166.
(45) Comby, S.; Bünzli, J.-C. G. In *Handbook on the Physics and Chemistry of Rare Earths*; Elsevier Science B.V.: Amsterdam, 2007; Vol. *37*, pp 217−470.
(46) Sun, L.-N.; Zhang, H.-J.; Yu, J.-B.; Yu, S.-Y.; Peng, C.-Y.; Dang, S.; Guo, X.-M.; Feng, J. *Langmuir* **2008**, *24*, 5500−5507.
(47) Ohishi, Y.; Kanamori, T.; Temmyo, J.; Wada, M.; Yamada, M.; Shimizu, M.; Yoshino, K.; Hanafusa, H.; Horiguchi, M.; Takahashi, S. *Electron. Lett.* **1991**, *27*, 1995−1996.
(48) Hsu, K.; Miller, C. M. *Opt. Lett.* **1994**, *19*, 886−888.
(49) Özen, G.; Denis, J. P.; Goldner, P.; Wu, X.; Genotelle, M.; Pellé, F. *Appl. Phys. Lett.* **1993**, *62*, 928−930.
(50) Jiang, F.-L.; Poon, C.-T.; Wong, W.-K.; Koon, H.-K.; Mak, N.-K.; Choi, C. Y.; Kwong, D. W. J.; Liu, Y. *ChemBioChem* **2008**, *9*, 1034−1039.
(51) Slooff, L. H.; Polman, A.; Cacialli, F.; Friend, R. H.; Hebbink, G. A.; van Veggel, F. C. J. M.; Reinhoudt, D. N. *Appl. Phys. Lett.* **2001**, *78*, 2122−2124.
(52) Lin, S.; Feuerstein, R. J; Mickelson, A. R. *J. Appl. Phys.* **1996**, *79*, 2868−2874.
(53) Feng, J.; Song, S.-Y.; Deng, R.-P.; Fan, W.-Q.; Zhang, H.-J. *Langmuir* **2010**, *26*, 3596−3600.
(54) Slooff, L. H.; de Dood, M. J. A.; van Blaaderen, A.; Polman, A. *Appl. Phys. Lett.* **2000**, *76*, 3682−3684.
(55) Monguzzi, A.; Tubino, R.; Meinardi, F.; Biroli, A. O.; Pizzotti, M.; Demartin, F.; Quochi, F.; Cordella, F.; Loi, M. A. *Chem. Mater.* **2009**, *21*, 128−135.
(56) Sun, L.-N.; Zhang, H.-J.; Fu, L.-S.; Liu, F.-Y.; Meng, Q.-G.; Peng, C.-Y.; Yu, J.-B. *Adv. Funct. Mater.* **2005**, *15*, 1041−1048.
(57) Dang, S.; Liu, Q.; Liu, K.; Guo, Z.; Sun, L.; Song, S.; Zhang, H. *Cryst. Growth Des.* **2010**, *10*, 4662−4667.
(58) Lo, J. W.; Lien, W. C.; Lin, C. A.; He, J. H. *ACS Appl. Mater. Interfaces* **2011**, *3*, 1009−1014.
(59) Polman, A.; van Veggel, F. C. J. M. *J. Opt. Soc. Am. B* **2004**, *21*, 871−892.
(60) Barbosa, A. J.; Dias Filho, F. A.; Maia, L. J. Q.; Messaddeq, Y.; Ribeiro, S. J. L.; Gonçalves, R. R. *J. Phys.: Condens. Matter* **2008**, *20*, 285−224.
(61) Slooff, L. H.; van Blaaderen, A.; Polman, A.; Hebbink, G. A.; Klink, S. I.; van Veggel, F. C. J. M.; Reinhoudt, D. N.; Hofstraat, J. W. *J. Appl. Phys.* **2002**, *91*, 3955−3980.
(62) Dang, S.; Yu, J. B.; Wang, X.; Sun, L. N.; Deng, R. P.; Feng, J.; Fan, W. Q.; Zhang, H. J. *J. Lumin.* **2011**, *131*, 1857−1863.
(63) Hong, Z.; Liang, C.; Li, R.; Zang, F.; Fan, D.; Li, W.; Hung, L. S.; Lee, S. T. *Appl. Phys. Lett.* **2001**, *79*, 1942−1944.
(64) Suga, J. *J. Opt. Soc. Am.* **1963**, *53*, 831−839.
(65) Foley, T. J.; Harrison, B. S.; Knefely, A. S.; Abboud, K. A.; Reynolds, J. R.; Schanze, K. S.; Boncella, J. M. *Inorg. Chem.* **2003**, *42*, 5023−5032.
(66) Law, G.-L.; Pham, T. A.; Xu, J.; Raymond, K. N. *Angew. Chem., Int. Ed.* **2012**, *51*, 2371−2374.
(67) Wartenberg, N.; Raccurt, O.; Bourgeat-Lami, E.; Imbert, D.; Mazzanti, M. *Chem.—Eur. J.* **2013**, *19*, 3477−3482.
(68) Dang, S.; Yu, J.; Yu, J. B.; Wang, X. F.; Sun, L. N.; Feng, J.; Fan, W. Q.; Zhang, H. J. *Mater. Lett.* **2011**, *65*, 1642−1644.
(69) Sun, L.-N.; Zhang, H.-J.; Meng, Q.-G.; Liu, F.-Y.; Fu, L.-S.; Peng, C.-Y.; Yu, J.-B.; Zheng, G.-L.; Wang, S.-B. *J. Phys. Chem. B* **2005**, *109*, 6174−6182.